Atmospheric CO_2 Sensing with a Random Modulation Continuous Wave Integrated Path Differential Absorption Lidar

Mathieu Quatrevalet, Xiao Ai, Antonio Pérez-Serrano, Pawel Adamiec, Juan Barbero, Andreas Fix, Jose Manuel G. Tijero, Ignacio Esquivias, John G. Rarity and Gerhard Ehret

***Abstract*—We propose an integrated path differential absorption (IPDA) lidar system based on a hybrid master oscillator power amplifier (MOPA) and single photon counting detection for column-averaged measurements of atmospheric CO_2. The random modulated continuous wave (RM-CW) approach has been selected as the best suited to the average output power obtained from hybrid and monolithically integrated MOPAs. A compact RM-CW IPDA lidar instrument has been designed and fabricated. High sensitivity and low noise single photon counting has been used for the receiver. Co-located 2 km horizontal trial path experiments with a pulsed system and in-situ measurements were performed for comparison. The RM-CW IPDA lidar instrument shows a relative accuracy of the order of about $\pm$10 % or $\pm$40 ppm CO_2 concentration in absolute terms. The measurements qualitatively demonstrate the feasibility of CO_2 IPDA measurements with a RM-CW system.**

I. Introduction

CARBON dioxide (CO_2) is the major anthropogenic greenhouse gas contributing to global warming and climate change. Due to gaps in the understanding of the carbon cycle, a better knowledge of the spatial and temporal distribution of the sources and sinks of CO_2 at the Earth's surface is required for appropriate policy-making. In the so-called top-down approach, the sources and sinks are inferred from the observed spatial gradients in the atmospheric CO_2 column concentration, making use of atmospheric transport models and the inverse modeling technique [1]. However, at present, the concentration is mainly measured in-situ at a number of surface stations that are very sparsely and unevenly distributed over the planet. While some passive instruments already provide global maps of the CO_2 column, they are prone to intereference from aerosols and thin clouds, and are typically not sensitive enough in the lowermost layer of the troposphere, where the gradients are the strongest [2], [3]. Futhermore they cannot provide measurements at high latitudes and during night time. Future space-borne active missions based on the integrated path differential absorption (IPDA) technique have the potential to overcome these limitations and close the gap [4], [5].

Typical laser sources currently used for gas sensing in IPDA systems (or its range-resolving counterpart, the differential absorption lidar (DIAL)) are solid state lasers (SSLs) working in pulsed regime. They emit ns pulses with high energy at low to medium repetition rate (typical values are 10-50 ns, $\sim$10-50 mJ, 50-200 Hz) [6]-[13]. These values correspond to $\sim$500 kW pulse peak power and $\sim$2 W of average power. Although these laser systems have demonstrated the characteristics required by the application, i.e. high average power, high laser beam quality and frequency stability, it is at the expense of a bulky system with low wall plug efficiency which is a main concern for space-borne applications.

Systems combining distributed feedback (DFB) semiconductor lasers or external cavity diode lasers (ECDLs) as seed lasers and erbium doped fiber amplifiers (EDFAs) have also been used to perform CO_2 measurements [14]-[18]. Although the use of active optical fibers in space applications requires specific attention due to their sensitivity to radiation, recent progresses have been made to develop high power EDFAs for different space applications [19], [20]. Average powers higher than 5 W and 20 W have been demonstrated in EDFAs for free space communications and IPDA lidar applications, respectively [21].

Approaches based on semiconductor lasers and amplifiers are promising candidates to be used in future air-borne and space-borne IPDA systems because they have clear advantages over other laser types in terms of compactness and conversion efficiency (up to 75 %). In addition, they present high reliability and good radiation hardness for most space applications In a very recent publication an attempt has been undertaken to use ECDLs and external semiconductor amplifiers for column measurements of CO_2 and methane (CH_4) [22]. The monolithically integrated master oscillator power amplifier (MOPA) architecture is particularly attractive due the small footprint and simplicity. These devices have reached output powers of

This work was supported by the European Commission through the project FP7-SPACE BRITESPACE under grant agreement no. 313200. A. Pérez-Serrano, J. M. G. Tijero and I. Esquivias also acknowledge support from the Ministerio de Economía y Competitividad of Spain under projects RANGER (TEC2012-38864-C03-02) and COMBINA (TEC2015-65212-C3-2-P); and the Comunidad de Madrid under program SINFOTON-CM (S2013/MIT-2790). A. Pérez-Serrano acknowledges support from Ayudas a la Formación Posdoctoral 2013 program (FPDI-2013-15740). P. Adamiec acknowledges support from the Torres Quevedo 2013 program (PTQ-13-06438).

M. Quatrevalet, A. Fix and G. Ehret are with the Institut für Physik der Atmosphäre, Deutsches Zentrum für Luft- und Raumfahrt (DLR) Oberpfaffenhofen, Münchner Straße 20, 82234 Weßling, Germany.

X. Ai ad J. G. Rarity are with the Dept. of Electrical and Electronic Engineering, University of Bristol, Merchant Venturers Building, Woodland Road, Bristol BS8 1UB, United Kingdom.

A. Pérez-Serrano, J. M. G. Tijero and I. Esquivias are with CEMDATIC-E.T.S.I. Telecomunicación, Universidad Politécnica de Madrid, Avda. Complutense 30, 28040 Madrid, Spain.

P. Adamiec and J. Barbero are with ALTER Technology, Calle de la Majada 3, 28760 Tres Cantos, Spain.

12 W in CW operation and 42 W in pulsed operation at 1064 nm [23]. At eye-safe wavelengths, around 1500 nm, full-semiconductor MOPAs have reached 1.6 W in CW operation and 2.7 W in pulsed operation [24]. In any case, their main drawback is that they can not produce the high energy pulses obtained with SSLs and required by the application.

The alternatives to the pulsed operation are the so-called intensity modulation continuous wave (IM-CW) techniques [25]. These techniques include sine wave CW [26] and random modulated CW (RM-CW) approach [27], also called pseudo-random noise (PRN) modulation. The main feature of these techniques is that average output power is more important than peak power, thus making possible to use a relatively low peak power laser such as a monolithically integrated MOPA. During the last years, CO_2 measurements have been performed using sine wave CW techniques [17], [28]. In particular, a lot of research has been performed by NASA, including the proposal and realization of advanced sine wave CW techniques [29]-[32]. In a RM-CW lidar a pseudo-random sequence is sent to the atmosphere and the received signal reflected from the target is correlated with the original sequence in order to retrieve the path length [33]. The RM-CW approach has been successfully applied to spatial aerosol profile measurements [34], cloud topographic measurements [35], underwater ranging and imaging [36] and atmospheric temperature and wind measurements [37]. RM-CW has also been used in IPDA measurements of atmospheric water vapor [38] and DIAL gas sensing [39]. However, only recently the technical requirements regarding spectral purity, beam quality and output power have been achieved by semiconductor lasers. A monolithically integrated three-section MOPA fulfilling these requirements has been demonstrated in [40]. In principle, the experiments described in this paper should have been performed with two three-section MOPAs. Unfortunately, this was not possible due to technical problems and the experiments were performed with a back-up system based on an hybrid MOPA. On the side of the receiver, high sensitivity and low noise single photon counting (SPC) techniques have been found to be the most suited for the application [41].

In this paper we report on the design and development of a RM-CW IPDA lidar system based on a hybrid MOPA and SPC for atmospheric CO_2 concentration measurement. A compact eye-safe prototype instrument has been fabricated and tested. The transmitter is based on two commercial DFB lasers, providing the on-line and off-line wavelengths close to the selected CO_2 absorption line around 1572 nm, and being frequency stabilized by an external opto-electrical feedback loop. Both CW optical outputs are externally modulated and then amplified by an EDFA. The receiver is based on an in-house developed single photon detector. Co-located horizontal 2 km trial path CO_2 measurements were performed and compared with measurements of the pulsed system CHARM-F [7] and an in-situ instrument. The obtained experimental results demonstrate the validity of RM-CW IPDA lidar systems for atmospheric CO_2 sensing.

In Section II the theoretical background of both IPDA systems (RM-CW and pulsed) is briefly summarized. The compact fabricated RM-CW IPDA lidar instrument design is detailed in Section III. The test campaign performed together with a pulsed IPDA lidar instrument and an in-situ device is described in Section IV. Special emphasis in given to the experimental methodology used to compare the results obtained from the different instruments. Section V describes and discusses the obtained results. Finally, the conclusions are drawn in Section VI.

II. Theoretical background

Air-borne and space-borne pulsed IPDA lidar systems estimate the column concentration of trace gases in the atmosphere by measuring the pulse echoes scattered back to the instrument by a hard target at the end of the optical path [4], which is a cloud top or the Earth's surface. The standard technique consists in transmitting sequentially a pair of laser pulses at different frequencies: the on-line frequency (ν_{on}) is close to the center of a CO_2 absorption line, and the off-line frequency (ν_{off}) is set away of the same absorption line. Both frequencies are close enough such that the two pulses exhibit different CO_2 absorption but all other contributors to the return signal strength (attenuation from thin clouds, aerosols and non-CO_2 molecules and reflectivity of the target) are spectrally flat at this scale. Fig. 1 (a) shows the CO_2 one-way optical depth seen from a space-borne instrument for a US standard atmosphere and on a 3 km horizontal path at ground level. Several theoretical studies have investigated in detail the choice of the absorption line and the exact position of the on-line and off-line wavelengths with respect to the absorption line [4], [42]. In this work, we used the wavelengths proposed in [43] around the CO_2 absorption line at 6361.2504 cm^{-1}.

In a RM-CW or PRN lidar [27], a pseudo-random bit sequence (PRBS) is transmitted to the atmosphere, as illustrated on the top in Fig. 1 (b) for the on-line wavelength. In [44] we have theoretically analyzed the performance of a RM-CW IPDA system with SPC. In the following we summarize only the most relevant expressions required for making comprehensible our experimental analysis and the reader is referred there for further details. We use the most basic M-sequence [27] and the fact that the cross-correlation of an N-bit PRBS $a[i] \in \{0,1\}$ with its bipolar sequence described by $\tilde{a}[i] = 2a[i]-1 \in \{-1,1\}$, only has a significant value at zero shifts and close to zero elsewhere. It can be written, for $N \gg 1$, as

$$a[i] \otimes \tilde{a}[i] \simeq \frac{N}{2}\delta[i] \ , \tag{1}$$

where $\delta[i]$ is the discrete unit impulse function or Kronecker delta ($\delta_{i,0}$). In the case of RM-CW IPDA systems a second PRBS originated from a second laser at the off-line frequency is simultaneously transmitted. The two signals share the same code but with a delay between them [45], [46]. The received signals, as illustrated in third and fourth rows of Fig. 1 (b) present a delay corresponding to the time-of-flight (TOF) with respect to the emitted sequences. The signal at the receiver, together with a fraction of the transmitted signals to be used as power reference, is correlated with the original sequence. The result of the cross-correlation shows four peaks in the correlation time scale, which are proportional to the transmitted and

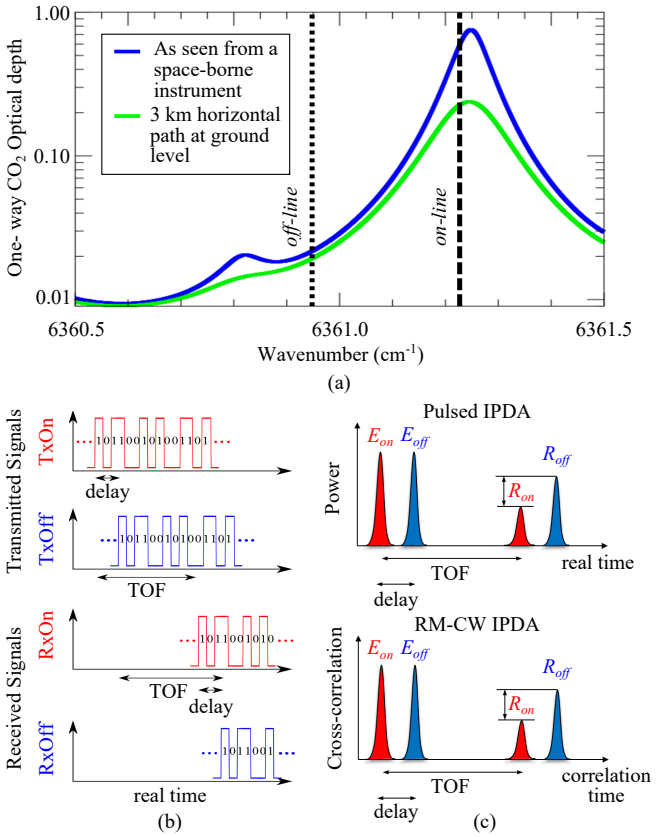

Fig. 1. (a) CO_2 one-way optical depth seen from a space-borne instrument (blue) for a US standard atmosphere and on a 3 km horizontal path at ground level (green) for a pressure of 1013.15 hPa and a temperature of 273.13 K (close to the temperatures encountered during the test campaign). The chosen CO_2 absorption line is at 6361.2506061 cm^{-1} (1572.01792843 nm) [43]. The on-line and off-line frequencies are indicated with black dashed and dotted lines, respectively. (b) Pseudo-random bit sequences (PRBS) used in the random modulated continuous wave (RM-CW) lidar approach. (c) Differential absorption optical depth ($DAOD$) measurement from the pulsed (top) and RM-CW (bottom) IPDA lidar systems. TOF: Time of flight.

received powers in both wavelengths. The peaks are separated by the delay and the TOF. This is illustrated in Fig. 1 (c), where the four peaks obtained in a pulsed system in a real time scale (top) are compared with the four cross-correlation peaks in the RM-CW system (bottom). The ratio between peaks provides information about the differential attenuation of the beam. In both cases, pulsed and RM-CW systems, the one-way differential atmospheric optical depth ($DAOD$) is the physical quantity that can be directly derived from the return signals R_{on} and R_{off} as

$$DAOD = \frac{1}{2}\ln\left(\frac{E_{on}}{E_{off}}\frac{R_{off}}{R_{on}}\right) \ , \tag{2}$$

where E_{on} and E_{off} are internal references at each wavelength. In the case of a pulsed system, $E_{on,off}$ are proportional to the transmitted energy pulses at on- and off-line wavelengths and $R_{on,off}$ are proportional to the number of photons scattered back from the hard target to the receiver. On the other hand in the case of a RM-CW system, $E_{on,off}$ are the cross-correlation peaks corresponding to the reference of the transmitted on- and off-line signals and $R_{on,off}$ are obtained from the peaks corresponding to the received echoes. In our case, using SPC, they can be written as [44]

$$R_{on,off} = NT_c\eta_e P_{on,off}\alpha\frac{A_r}{D^2}e^{-2OD_{on,off}} \ , \tag{3}$$

where T_c is the bit time or chip time, η_e denotes the conversion coefficient from total photon energy to detections of photo-electrons, $\eta_e = \lambda\eta_{ph}/(hc)$, where λ is the emission wavelength, η_{ph} is the optical and quantum efficiency, h is the Planck's constant and c is the speed of light in vacuum; $P_{on,off}$ are the emitted average power at each sounding wavelength, α is the surface albedo or target reflectivity, A_r is the area of the receiver, D is the distance to the target and

$$OD_{on,off} = OD_0 + \int_0^D \sigma_{on,off}(p,T)n_{co2}(p,T)\ dz \ , \tag{4}$$

is the total column optical depth, which includes a frequency-independent losses term due to aerosols OD_0, and the CO_2 optical depth, where $p = p(z)$ and $T = T(z)$ are the pressure and temperature profiles along the path, $\sigma_{on,off}(p,T)$ are the pressure- and temperature-dependent absorption cross-sections of CO_2 at each wavelength and $n_{co2}(p,T)$ is the CO_2 number density. Making use of the Beer-Lambert law along the laser beam, the $DAOD$ can be converted to a weighted average of the dry-air volume mixing ratio of CO_2 along the laser beam, XCO_2, the quantity of scientific interest,

$$XCO_2 = \frac{DAOD}{IWF} \ , \tag{5}$$

with

$$IWF = \int_0^D \left[\sigma_{on}(p,T) - \sigma_{off}(p,T)\right] n_{air}(p,T)\ dz \ , \tag{6}$$

being the integrated weighting function, where $n_{air}(p,T)$ is the dry air number density, which is related to $n_{co2}(p,T)$ via the volume mixing ratio $vmr_{co2}(p,T) = n_{co2}(p,T)/n_{air}(p,T)$. Thanks to spectroscopic characterizations of the absorption cross-section in the laboratory and pressure and temperature profiles from a weather station or a numerical weather prediction model, Eqs. (5) and (6) are typically applied for a down-looking, space-borne or air-borne instrument.

In the case of RM-CW SPC IPDA lidar, the signal to noise ratio (SNR) can be written as [44]

$$SNR_{on,off} = \frac{R_{on,off}}{\sqrt{R_{on} + R_{off} + R_{det} + R_{amb}}} \tag{7}$$

where R_{det} takes into account the detector dark counts, $R_{det} = Nk_{dc}T_c$, being k_{dc} the dark count rate per second; and R_{amb} represents the shot noise induced by the ambient light,

$$R_{amb} = NL_s\eta_e T_c\Delta_\lambda A_s\frac{A_r}{D^2}e^{-OD_0} \ , \tag{8}$$

where L_s is the solar spectral radiance, Δ_λ is the filter bandwidth and A_s is the target surface area covered by the detector field-of-view (FOV), $A_s = \pi\theta_{FOV}^2 D^2/4$. A deep analysis of the previous equations including parameter dependence in the context of a space-borne scenario can be found in [44]. Our results indicated that a worst case retrieval precision of

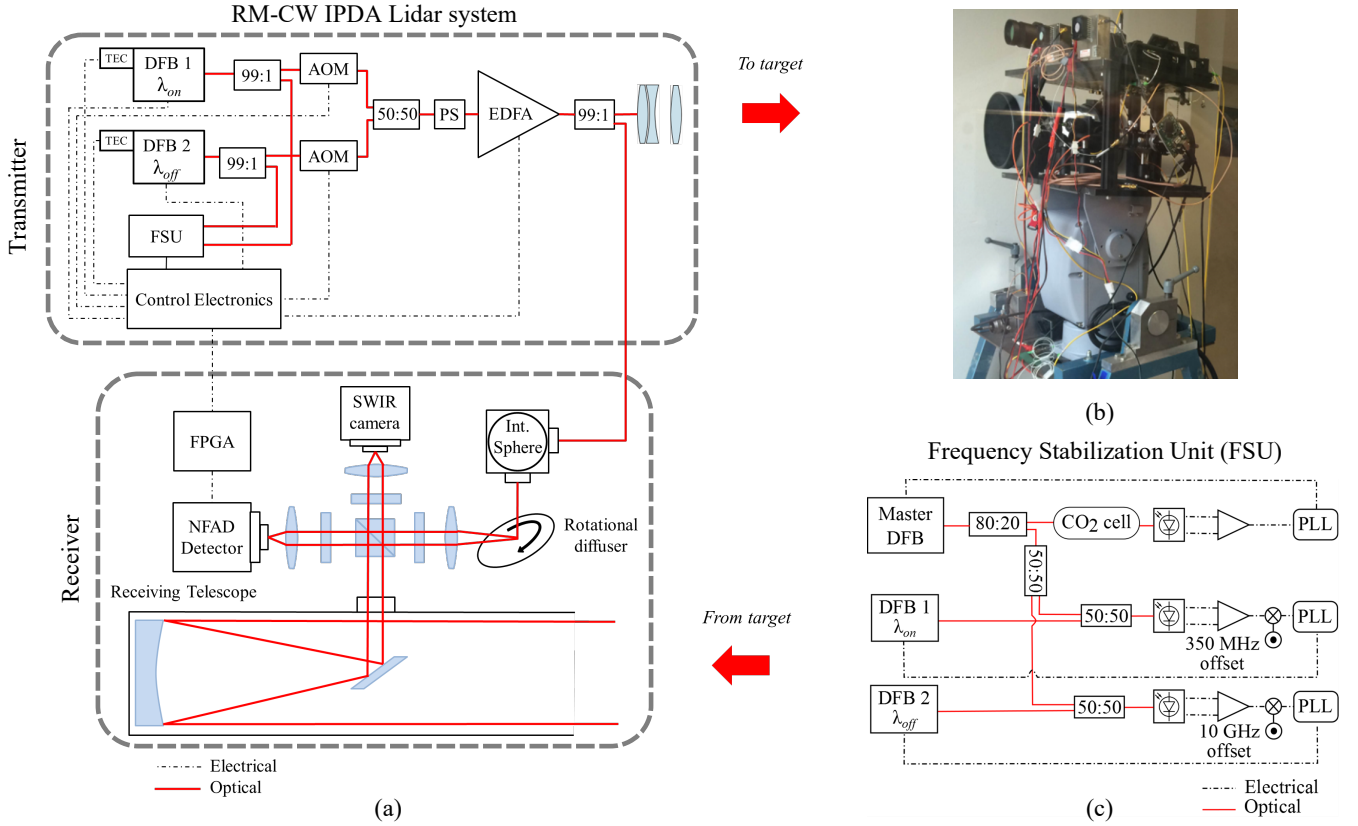

Fig. 2. (a) Schematics of the RM-CW IPDA lidar system composed by the transmitter (top) and the receiver (bottom). DFB: Distributed feedback laser. TEC: Thermo-electric cooler. AOM: Acousto-optic modulator. EDFA: Erbium doped fiber amplifier. FSU: Frequency stabilization unit. PS: Polarization scrambler. NFAD: Negative feedback avalanche diode. SWIR: Short-wave infrared. FPGA: Field programmable gate array. (b) Photograph of the fabricated RM-CW IPDA lidar instrument. (c) Schematics of the FSU, based on three phase locking loops (PLLs).

1.5 ppm over a 50 km path integration can be obtained for expected conditions in a space mission assuming state-of-the-art photon counting detectors and transmitters delivering an average output power of 2 W.

III. RM-CW IPDA LIDAR SYSTEM

The design of the complete IPDA lidar system is shown in Fig. 2 (a). It consists of the laser transmitter, the optics for beam transmission and reception, and the control electronics. The laser transmitter architecture is shown in the upper part of Fig. 2 (a). It provides two output beams: one is sent to the target and the other is used as reference and mixed with the received signal, for the calculation of the $DAOD$. It consists of two DFB lasers (one for each sounding frequency λ_{on}, λ_{off}), two acousto-optic modulators (AOMs), an EDFA, the control electronics and the frequency stabilization unit (FSU). A fraction of the output power of the two laser chips is sent to the FSU in order to stabilize the emission frequency. The other fraction is sent to an AOM where is non-return-to-zero (NRZ) modulated with the PRBS. We have used a chip time $T_c = 40$ ns corresponding to a bit rate of 25 Mb/s, thus the range resolution of the system is 6 m. The length of the PRBS is $N = 2^{14} - 1 = 16383$, therefore the unambiguous range is 98.3 km. After the AOM, the two signals are combined and sent to a polarization scrambler (PS) avoiding the polarization dependent beam splitting to the reference path before being amplified by the EDFA (Keopsys KPS-STD-BT-L-30-PB-101-FA-FA). The average output power for each sounding frequency after the amplification stage is around 0.3 W. After being amplified a small fraction of the signal is sent to the integrated sphere to be used as reference by the receiver. The integrating sphere is used for beam homogenization and the rotational diffuser reduces the speckle noise in the references. One should notice that there is also another speckle noise source that affect our measurements. The one that comes from the target, due to fixed or slowly moving target. This can be minimized by vibrating or moving the transceiver [22], and it will not be present in air-borne or space-borne systems when target (lidar) is moving at high speed. In our case the pan-tilt mounting allowed to vibrate the instrument, in order to slightly but continuously change the line-of-sight of the whole instrument, thereby changing the speckle pattern at the target. Fig. 2 (b) shows a photograph of the compact fabricated instrument on the mount.

For accurate estimation of the gas molecule concentration, IPDA lidar systems require high frequency stabilization [4]. In this regard, the most critical frequency is the on-line, due to the slope in the wing of the line. The CW emission linewidth and the linewidth knowledge accuracy are expected to be uncritical for the proposed transmitter, because pseudo-random modulation dominates the linewidth. The expected broadening at full width at half maximum (FWHM) in our system is

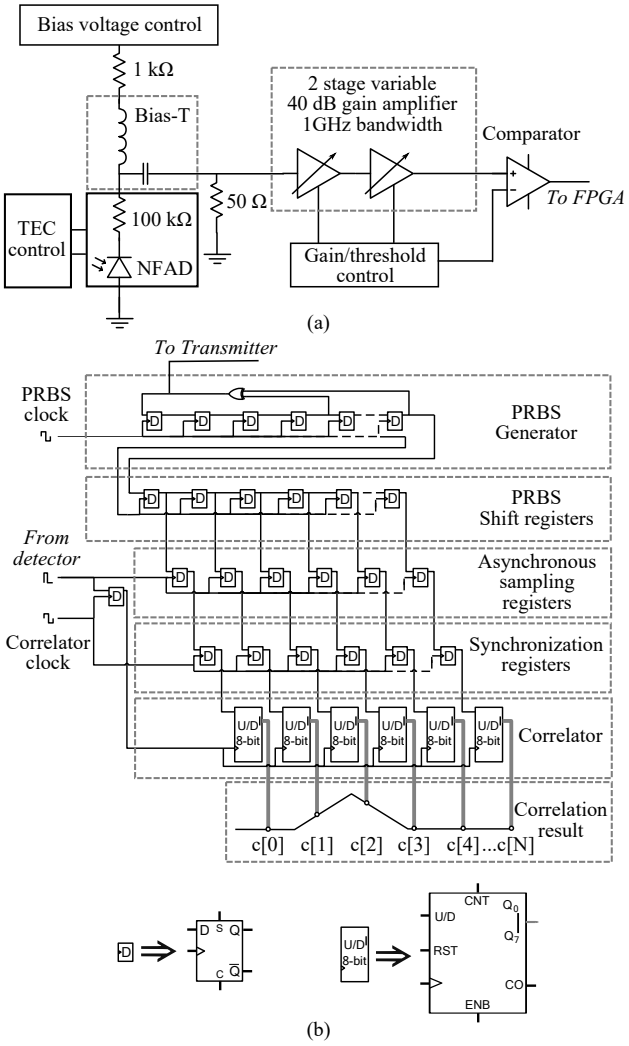

Fig. 3. (a) Schematics of the in-house developed single photon counting (SPC) detector based on a NFAD. (b) FPGA asynchronous implementation of the PRBS generator and correlator, composed by D flip-flops and up/down (U/D) 8 bit counters.

around 25 MHz (twice the data rate); this broadening can be characterized and since it is reproducible it can easily be corrected during data processing. In this work, we did not correct for this effect. In order to achieve the frequency stability requirements, we use two opto-electrical feedback loops, based on phase locking loops (PLLs) (LaseLock 4 Channel), for the stabilization of the on- and off-channels coupled to the output of a third opto-electrical feedback loop for CO_2 locking. The scheme of the FSU is shown in Fig. 2 (c). Light emitted from the on-line DFB laser is sent to the on-line locking feedback loop. In the same way, the light emitted from the off-line DFB laser is sent to the off-line locking feedback loop. We use a master DFB laser that is locked to the selected CO_2 absorption line using a single pass CO_2 reference cell and a custom feedback loop based on a commercially available laser frequency locking equipment. The measured master DFB stabilization range is around 18 kHz at the interval of 23 s, thus marking a limit on the on- and off-line wavelengths. The light emitted from the master laser is injected into the on- and

TABLE I
RM-CW IPDA LIDAR SYSTEM PARAMETERS

Transmitter		
On-line average output power	P_{on}	300 mW
Off-line average output power	P_{off}	300 mW
On-line frequency	ν_{on}	190.704710 THz
Off-line frequency	ν_{off}	190.694980 THz
PRBS chip time	T_c	40 ns
Length sequence	N	16383
Beam divergence	θ_{div}	200 μrad
Receiver		
Telescope mirror area	A_r	1.82×10^{-2} m^2
Receiver field-of-view	θ_{FOV}	200 μrad
Dark count rate	k_{dc}	100 kcps
Optical and quantum efficiency	η_{ph}	10 %
Sampling rate		100 MS/s

off-line frequency locking loops and it is used to stabilize the beat note of the on-line and off-line signals with respect to the master laser frequency, with a tunable 350 MHz and with a fixed 10 GHz offsets, respectively. We measured a stability of $\sim$50 kHz during 20 s for the off-set locked lasers.

On the side of the receiver, the reflected light from the target is collected by a Newtonian telescope ($\oslash$ = 152.4 mm) with a field of view (FOV) of 200 μrad matching the laser beam divergence. Alignment issues are addressed by using a short-wave infrared (SWIR) camera. A very high sensitivity detector based on InGaAs negative feedback avalanche diode (NFAD) is used for SPC of the received signal. The NFAD is used in order to minimize the degradation of the SNR in comparison with pulsed systems due to the detector noise [41]. We have developed in-house our own single photon detector unit as commercial detectors do not satisfy our need of a high saturation count rate [47]. A scheme of the single photon detector is plotted in Fig. 3 (a). The detector achieves 5 Mcps with 100 kcps dark count with an efficiency of 10 %. It should be noticed, that the intrinsic NFAD non-linearity caused by detector dead-time can be completely canceled out, due to the fact that CO_2 concentration is calculated from the ratio between the on- and off-line received echoes [41].

The modulation sequence and the correlation process required by the RM-CW technique are implemented with a field programmable gate array (FPGA). Alternatively to other correlators, the FPGA implementation of the single photon correlator is based in an asynchronous design, see Fig. 3 (b). This presents modifications respect to the correlators presented in [33], [48]. First of all the PRBS is generated by a first layer of linear feedback shift registers. A second layer of shift registers, acting as delay lines, records the PRBS signal. Once a photon is received, the rising edge of the photon trigger will latch the shift register contents into the flip-flop of the asynchronous sampling registers. Subsequent to this layer a synchronization registers layer is needed to deal with meta-stability. The last layer is the correlator elements that are just counters which increments with logic '1' being seen at the second layer shift registers and decrement with '0'. The result of the correlation appears as a triangle (see Fig. 3 (b)) where

the addition of the two highest consecutive peaks (c[1] and c[2]) indicate the number of correlated photons. The optical spectra of the on-line signal will be distorted due to its position on the wing of the absorption line, and consequently also the temporal response. This effect will influence the shape of the correlated signal, but it will not generate distortion or side-lobes in the correlation result. The shape of the correlated peak is not important, only the total energy within the correlation peak is considered. Table I shows a summary of the RM-CW IPDA lidar system parameters.

IV. Measurement scenario and methodology

In order to test and demonstrate the validity of the RM-CW IPDA lidar system for column-averaged CO_2 concentration measurement, a test campaign with co-located measurements with a pulsed system and an in-situ instrument was performed. The test campaign took place during February 2016 at the Institute of Atmospheric Physics, DLR Oberpfaffenhofen, Germany. In the following subsections, details on the pulsed system, the trial path and the experimental methodology are given.

A. CHARM-F system overview

CHARM-F is the result of a five-year in-house development [7], [49], [50], which aims to serve as a technology demonstrator for IPDA lidar measurements of the two main anthropogenic greenhouse gases, CO_2 and CH_4. The instrument was designed to fly on a research aircraft in a down-looking configuration, but can also be operated from the ground in a sideways-looking configuration thanks to a dedicated frame. CHARM-F's laser sources (one for CO_2 and the other for CH_4) are based on injection-seeding of pulsed optical parametric oscillators (OPO) by a low-power, CW laser source, allowing to simultaneously achieve the very narrow bandwidths and high pulse energies required for the application. The OPOs are themselves pumped by Nd:YAG lasers producing double pulses at 1064 nm separated by only a few hundred ns at a rate of 50 Hz. A fast optical switch enables switching between the on-line and off-line seed laser in the short time between the two pulses. The spatial mismatch between on-line and off-line footprint on ground is thereby minimized, although not fully removed. In this aspect the RM-CW approach presents a clear advantage.

The OPO cavity must be actively maintained in resonance with the seed lasers by means of a piezoelectric actuator on one of the cavity mirrors; a heterodyne measurement of the frequency difference between a frequency-shifted (by means of an AOM) light from the seed laser and a very small fraction of the outgoing OPO pulses, picked up by a fiber, provides the error signal.

Fig. 4 (a) shows both instruments in the laboratory, the RM-CW IPDA lidar and the CHARM-F system in its frame and the rack for the frequency reference and data acquisition subsystems. CHARM-F is equipped with two receivers per trace gas, one making use of a quadrant PIN photodiode and a reflective telescope with an aperture of 20 cm, the other making use of an avalanche photodiode (APD) at the focus of a refractive telescope of 6 cm aperture. The APD and small telescope were designed to mimic the configuration that would be favoured for a spaceborne instrument, while the quadrant PIN photodiode allows active beam pointing on the one hand, and cross-checks of the APD-retrieved values, as discussed in Section V. Unfortunately, the CHARM-F lasers themselves were not used during the experiments due to issues with the pump units. However, a back-up was available in the form of an early OPO prototype pumped by a commercial double-pulse Nd:YAG laser on the optical table of the laboratory (not shown). The OPO output energy was of the order of 2.5 mJ per pulse, which provided a sufficient SNR on the trial path described hereafter. The output laser beam from the prototype was guided to the CHARM-F optical bench, and the relevant electronic and optical signals for injection seeding and OPO cavity stabilization were brought to and from the frequency stabilization and data acquisition unit.

B. Trial path and in-situ instrument

DLRs premises in Oberpfaffenhofen are placed in a rural setting, right next to an airfield, and thanks to a convenient position of the Institute with respect to the neighboring buildings, one window of the laboratories offers an obstacle-free view across the airfield to a forested area at a distance of around 2 km, as illustrated on Fig. 4 (b). Furthermore, the presence of a hill on the line of sight makes it possible to target trees at different ranges, from about 2 to 3 km. This trial path was previously used successfully for the validation of IPDA systems [7].

The in-situ instrument (LI-820 CO_2 gas analyzer) is based on a dual filter infrared detection system. By means of a long plastic pipe and existing feedthroughs between the laboratory and an astronomical cupola on the roof of the institute, the air was sampled directly above the lidar systems, as shown in Fig. 4 (c), providing a localized point measurement at the very beginning of the path. Since the building does not house a heating station, this location was optimal to ensure that no nearby source, such as an open window leaking office air, disturbs the measurement of the background concentration. However, local sources within a radius of a few tens to a few hundred meters still have an influence.

C. Methodology

As explained in the previous section, the measurements shown in this paper were performed in an horizontal path. In this case, Eq. (6) is greatly simplified compared to a down-looking IPDA measurement through many heterogeneous layers of the atmosphere. It can indeed be safely assumed that the pressure and temperature along the horizontal path are uniform, so Eq. (5) simplifies as

$$XCO_2 = \frac{DAOD}{D\left[\sigma_{on}(p,T) - \sigma_{off}(p,T)\right] n_{air}(p,T)} \,. \qquad (9)$$

In the frame of the measurements presented in this paper, the absorption cross-sections were computed using a Voigt profile and the latest line-by-line spectroscopic parameters from the HITRAN database [51]. Pressure and temperature

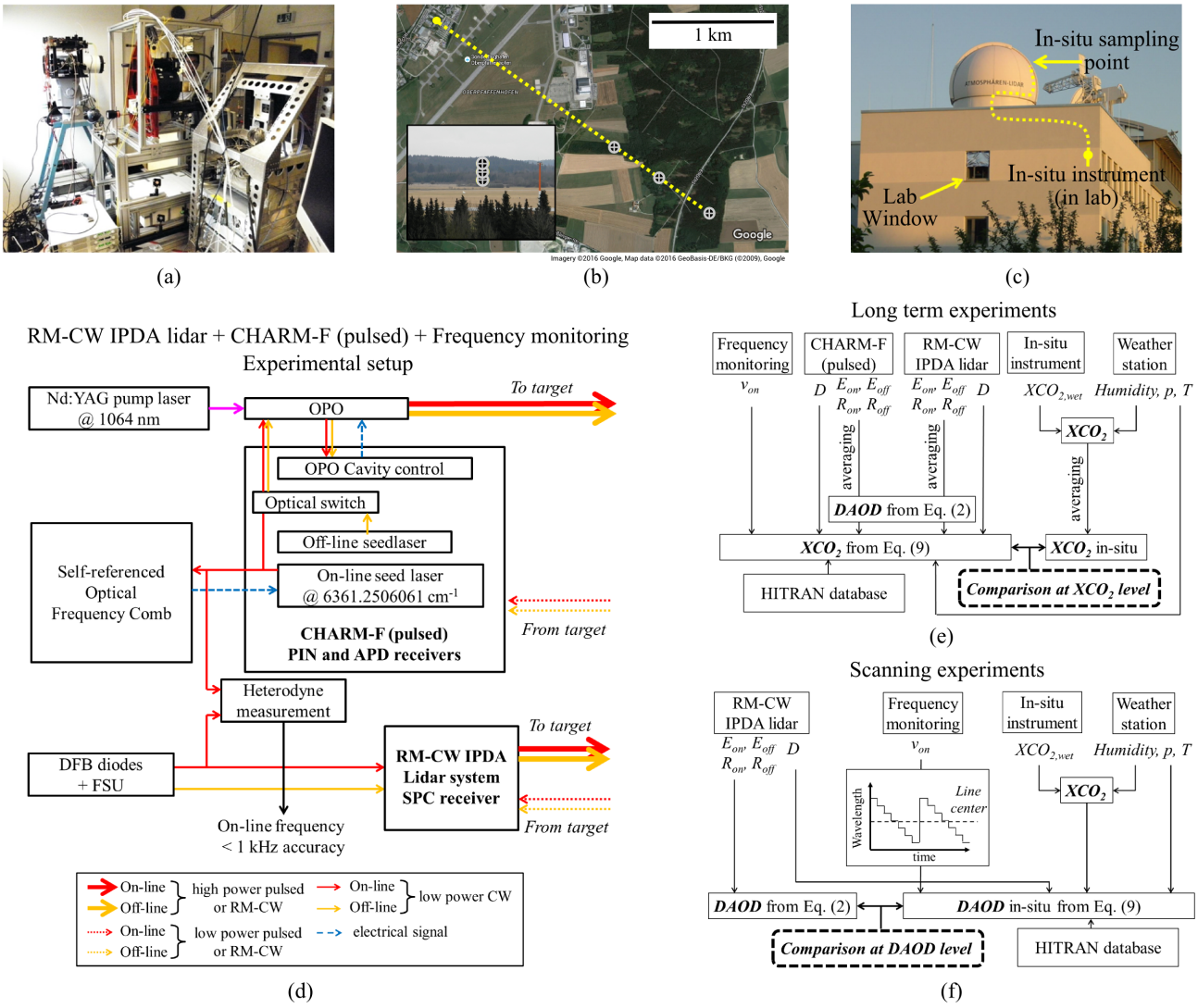

Fig. 4. Measurement scenario and methodology. (a) Photograph of the RM-CW IPDA lidar and CHARM-F instruments in the laboratory. The optical table containing the OPO back-up system and the self-referenced optical frequency comb (OFC) are not shown. (b) Map showing the trial path. The 2, 2.5 and 3 km path distances are indicated. Inset: view from the laboratory window. (c) Position of the in-situ instrument and the laboratory window where lidar instruments are located. (d) Experimental setup consisting in both systems, the RM-CW IPDA and CHARM-F instruments, and the OFC. (e) and (f) Diagrams of the long term and scanning experiments, respectively.

were measured by an autonomous weather station permanently installed on the building's roof.

Two type of experiments were performed, we refer to them as: (1) *long term experiments* and (2) *scanning experiments*. In the *long term experiments*, the three instruments were measuring simultaneously, both IPDA lidar instruments along the trial path but not at the same range. The nearest part of the forested area visible on the inset of Fig. 4 (b) - just over 2 km away - was used with the RM-CW system, while the pulsed system was pointed to the higher part of the forest, on top of the hill, at a distance of just under 3 km.

The experimental setup is shown in Fig. 4 (d). It consists of both lidar systems, the RM-CW IPDA and CHARM-F instruments, and a self-referenced optical frequency comb (OFC) (Menlo systems FC1500 Optical Frequency Synthesizer) with absolute long-term optical frequency stability better than 1 kHz, used for frequency monitoring and locking. Fig. 4 (e) shows a diagram explaining the method to perform the *long term experiments*. For both lidars, the $DAOD$ was calculated according to Eq. (2), from pulse energy or correlation measurements respectively. This value was then converted to XCO_2 using Eq. (9). To reach a sufficient SNR, averaging was applied in the form of a gliding average on the data. In order to avoid biases due to the low SNR at signal level and the non-linearities of Eq. (2), averaging was partly applied to the signals themselves, and partly to the ratio inside of the logarithm function, before the latter was applied. Eq. (9) was applied on the fully averaged (but still with the full original time resolution) data. In all of the results presented in Section V, the overall averaging time was 10 minutes.

As far as on-line and off-line wavelengths are concerned, the conditions were the following. The CHARM-F on-line

seed laser was locked to the self-referenced OFC using a PLL loop, effectively transferring the OFCs long-term stability to the on-line position. More specifically, the seed laser was first coarsely brought less than 30 MHz away from the top of the CO_2 absorption line at 1572.02 nm thanks to a high-accuracy wavemeter, calibrated using an acetylene-stabilized auxiliary laser. Then the repetition rate of the OFC was adjusted until the beat frequency between seed laser and OFC was close to 21.4 MHz, the center frequency of a bandpass filter used in the PLL electronics. The PLL, using a reference synthesizer at the same frequency, could then be switched on. From the repetition rate and the coarse ($<$ 30 MHz) knowledge of the seed laser position, the number of the OFC mode with which the seed laser was beating was determined, which enabled in turn to calculate the absolute optical frequency of the locked seed laser. This was 6361.2506061 cm^{-1}, i.e. only about 6 MHz away from the line center in vacuum (at 6361.250433 cm^{-1}, according to the latest HITRAN database) and it remained fixed for all of the measurement campaign.

The OFC-locked CHARM-F seed laser was used simultaneously as reference laser for monitoring the absolute position of the RM-CW IPDA lidar on-line laser when the latter was not locked using the FSU, using an heterodyne measurement technique. The frequency variations of the free-running (i.e. only temperature and current-regulated) on-line DFB laser of the RM-CW IPDA system were recorded for the 17/02. Over the whole afternoon, the laser drifted by less than 150 MHz peak-to-peak, which is only a fraction of the approximately 2.5 GHz-wide CO_2 absorption line at ground pressure. Since all measurements were carried out close to the top of the line, the corrections are rather subtle, but they were nevertheless taken into account in Eq. (9) when the on-line laser of the RM-CW IPDA system was not locked. On the in-situ instrument side, the same gliding average was applied on the XCO_2, and the values compared with the lidar retrievals from Eq. (9) for both instruments, and for both receivers in the case of CHARM-F.

In the second type of experiments, the *scanning experiments*, the RM-CW IPDA lidar system and the in-situ device results were compared. In this case steps were applied to the temperature regulation of the free-running RM-CW IPDA on-line DFB laser, so as to measure the $DAOD$ at different positions around the center of the absorption line. A diagram explaining the experiment is shown in Fig. 4 (f). The position at each step was held for about half a minute before applying the next step and ten steps were applied before going back to the initial position. The 10-step scan was repeated 10 times during each scanning experiment. In order to increase the SNR, the data at each step were averaged to provide a single point. Only Eq. (2) was applied, since the goal was to observe the absorption line's shape and compare with the expected values. The latter were calculated by applying the reverse of Eq. (9) from the in-situ device's data, using the knowledge of the on-line laser's absolute position and of the range. Although the frequency variations of the on-line laser during the hold time of each step were small, they were taken into account when computing the expected values.

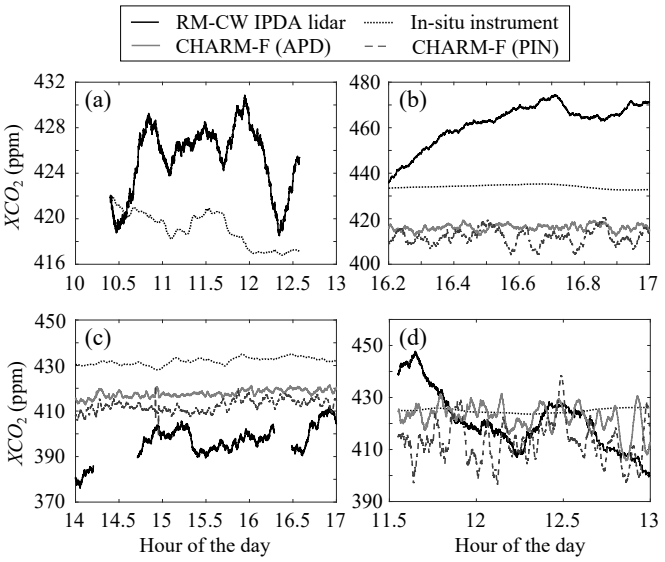

Fig. 5. Results of the long term experiments. CO_2 dry-air volume mixing ratio along the laser beam (XCO_2) measured with the different instruments: RM-CW IPDA lidar, in-situ instrument and CHARM-F. (a) 05/02/2016: $T = 278$ K and $p = 957$ hPa. (b) 16/02/2016: $T = 275$ K and $p = 958$ hPa. (c) 17/02/2016: $T = 275$ K and $p = 945$ hPa. (d) 18/02/2016: $T = 276$ K and $p = 946$ hPa.

V. Experimental results

Several series of long term and scanning experiments were performed in different days. Due to various issues with the weather (including intermittent snowfall on the 17/02) and with the systems, the maximum measurement duration with both instruments running was between one and three hours. Fig. 5 (a) compares the measured XCO_2 with the RM-CW IPDA system and the in-situ instrument during the first phase of the test campaign at the beginning of February, when the back-up laser for CHARM-F was not yet ready. The on-line laser of the RM-CW IPDA system was locked using the FSU. This experiment achieved the best match between the RM-CW IPDA system and the in-situ measurements, with a maximum discrepancy of 10 ppm over two hours.

During the measurement on the 16/02 (see results in Fig. 5 (b)), the pan-tilt vibration of the RM-CW IPDA system, which was intended to reduce the impact of speckle effects, was unintentionally switched off and the system displayed strong drifts. On the 17/02 and on the 18/02 (see results in Fig. 5 (c) and (d), respectively), the pan-tilt vibration was active but the results of the RM-CW IPDA system displayed some strong time-varying offsets in comparison with both the in-situ instrument and the CHARM-F data. These data were rather flat, except on the 18/02 for the CHARM-F.

Overall, time-varying offsets of up to ± 10 % were observed on the RM-CW IPDA system results with respect to the in-situ data. Offsets were also present in the data of the pulsed system; however, both receivers of the CHARM-F had a small and roughly constant offset relative to each other of about 10 ppm and a constant offset of -20 ppm with respect to the in-situ instrument data, while the RM-CW IPDA system had a different offset (with a different sign) on different days. The

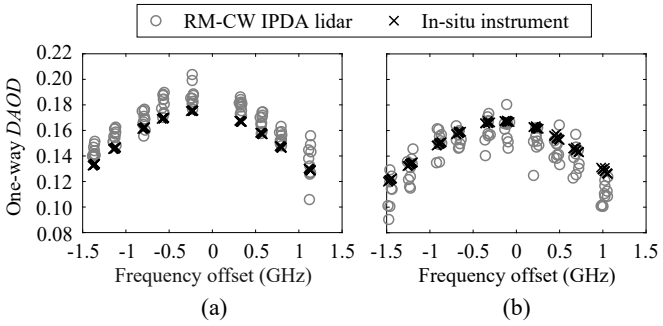

Fig. 6. Results of the scanning experiments. The one-way differential absorption optical depth ($DAOD$) versus frequency offset with respect to the CO_2 line center in vacuum, measured with the RM-CW IPDA lidar and the expected values derived from the in-situ instrument. (a) 16/02/2016. (b) 17/02/2016.

constant offset can be satisfyingly explained by the uncertainty of ± 10 ppm on the concentration of CO_2 in the reference mixture that was used to calibrate the in-situ instrument, on the one hand, and by the uncertainties in the HITRAN line parameters that were used to convert between XCO_2 and $DAOD$ values through Eq. (9), on the other hand.

As far as the remaining variations are concerned, some evidence points to speckle effects combined with the heterogeneous reflectivity of the target. First, the CHARM-F data exhibits larger instability on the 18/02, when the local wind was weaker than on the previous days, producing less "blurring" of the speckle patterns through the movement of the trees. Second, a faster drift of the RM-CW system is observed on the 16/02, when the pan-tilt motion of the system, meant to introduce speckle diversity by changing the line-of-sight, was unintentionally switched off. And third, the generally larger amplitude of the variations on the RM-CW system are consistent with a smaller number of speckles in the field of view, due to the system's smaller divergence.

On the other hand, two exploitable scanning experiments were carried out during the measurement campaign, on the 16/02 and 17/02. The results are presented on Fig. 6 (a) and (b), respectively. The correct overall shape and position was obtained, with a shift of the absorption line at ground pressure of about 200 MHz towards lower optical frequencies with respect to the line center in vacuum, as expected. However, the same variability of about ± 10 % in the absolute values of the measured $DAOD$ was observed when comparing measurements at the same frequency position within the same scan experiment (as seen from the spread of the measurements within a column). A different overall offset from one experiment to the next was also observed: most measurements were above the expected value on the 16/02, but below the expected value on the 17/02.

After the evaluation of the accuracy of both IPDA lidar systems, we briefly analyze here the precision of the RM-CW IPDA lidar. Fig. 7 (a) shows, as an example, $DAOD$ measurements taken every 0.02 s corresponding to the 05/02/2016 data shown in Fig. 5 (a). The $DAOD$ Allan deviation of this data is shown in Fig. 7 (b). It is clear that up to $\sim$100 s the system is limited by shot noise. The precision of the one-

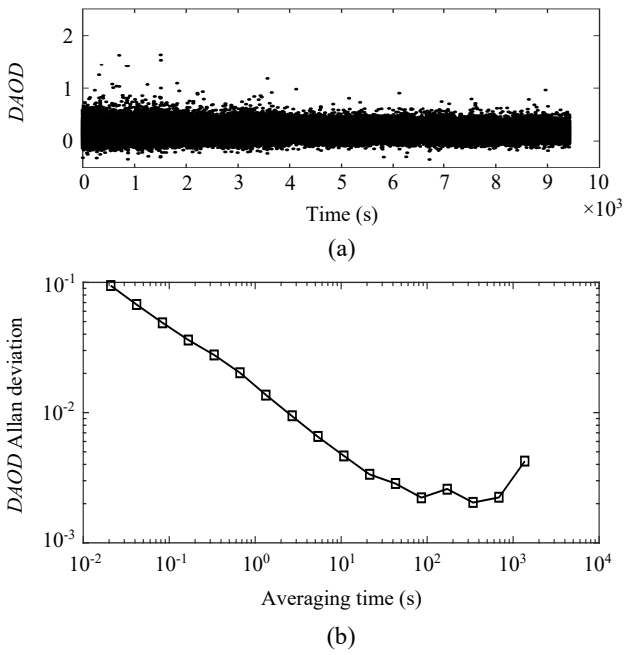

Fig. 7. Precision of the RM-CW IPDA lidar system. (a) $DAOD$ measurements for 10^4 s. The sampling time is 0.02 s. (b) $DAOD$ Allan deviation. Data corresponding to the measurements performed 05/02/2016, shown in Fig. 5 (a).

way $DAOD$ achieved in an integration time of 7 s (proposed for space-borne system) is 0.63 %, which corresponds to an XCO_2 error of 2.5 ppm. Speckle noise starts to dominate for integration times longer than 100 s. This result is not far from the error estimation making use of the theoretical SNR Eq. (7), although a direct comparison is difficult due to the uncertainties in some parameters, specially in the surface reflectivity. A more detailed comparison between theory and experiments is in progress and it will be further reported. The precision of the RM-CW instrument is comparable with other IPDA systems: Spiers et al. [9] reported a precision of 0.7 %, Kameyama et al. [14] estimated an statistical error of 4 ppm for 32 s measurements intervals, Dobler et al. [17] obtained values of 1.3 ppm over water and 0.97 ppm over land for 10 s averaging, and recently Wagner and Plusquellic [22] reported an error of 7 ppm for an integration time of 7 s. The error of our RM-CW instrument also compares well with that obtained for CHARM-F system on air-borne experiments where a statistical error of 0.7 % (2.8 ppm) was obtained.

VI. Conclusions

An IPDA lidar system for atmospheric CO_2 measurement based on a hybrid MOPA and SPC receiving techniques has been proposed and demonstrated. Experiments in a horizontal path have been carried out and compared with a pulsed system and with an in-situ instrument. It has been found that a relative accuracy of the order of about ± 10 %, or ± 40 ppm CO_2 concentration in absolute terms, was achieved with the proposed RM-CW IPDA lidar system. These numbers are more than one order of magnitude away from the threshold requirement for a space-borne IPDA lidar mission for CO_2,

however they should be put in perspective with the consideration that due to speckle effects, a horizontal measurement on a fixed target is a worst-case scenario compared to an air-borne or space-borne measurement with a continuously changing target. Our results have also shown than for a 7 s integration time, the random error in the $DAOD$ is about 0.67 %, corresponding to an XCO_2 error of 2.5 ppm. Nevertheless, our experiments qualitatively demonstrate the feasibility of CO_2 IPDA measurements with a RM-CW system. These systems can be implemented with recently demonstrated monolithically integrated MOPAs [40] together with SPC at the receiver for future space-borne lidar instruments.

ACKNOWLEDGEMENT

The authors would like to thank M. Faugeron, M. Krakowski and F. van Dijk at III-V Lab for the loan of the EDFA used in the RM-CW IPDA lidar instrument.

REFERENCES

[1] S. Houweling *et al.*, "Inverse modeling of CO_2 sources and sinks using satellite data: a synthetic inter-comparison of measurement techniques and their performance as a function of space and time," *Atmos. Chem. Phys.*, vol. 4, no. 2, pp. 523–538, 2004.

[2] K. Hungershoefer *et al.*, "Evaluation of various observing systems for the global monitoring of CO_2 surface fluxes," *Atmos. Chem. Phys.*, vol. 10, no. 21, pp. 10 503–10 520, 2010.

[3] S. Houweling *et al.*,"Evidence of systematic errors in SCIAMACHY-observed CO_2 due to aerosols,"*Atmos. Chem. Phys.*, vol. 5, no. 11, pp. 3003–3013, 2005.

[4] G. Ehret *et al.*, "Space-borne remote sensing of CO_2, CH_4, and N_2O by integrated path differential absorption lidar: a sensitivity analysis," *Appl. Phys. B*, vol. 90, no. 3, pp. 593–608, 2008.

[5] P. Ingmann, P. Bensi, and Y. Durand, *Candidate Earth Explorer Core Missions - Reports for Assessment: A-SCOPE Advanced Space Carbon and climate Observation of Planet Earth*, ESA SP-1313/1, ISBN 978-92-9221-406-7, ISSN 0379-6566, 2008

[6] G. J. Koch *et al.*, "Coherent differential absorption lidar measurements of CO_2," *Appl. Opt.*, vol. 43, pp. 5092-5099, 2004.

[7] A. Amediek, A. Fix, M. Wirth, and G. Ehret, "Development of an OPO system at 1.57 μm for integrated path dial measurement of atmospheric carbon dioxide," *Appl. Phys. B*, vol. 92, no. 2, pp. 295–302, 2008.

[8] D. Sakaizawa *et al.*, "Development of a 1.6 μm differential absorption lidar with a quasi-phase-matching optical parametric oscillator and photon-counting detector for the vertical CO_2 profile, *Appl. Opt.*, vol. 48, no. 4, pp. 748–757, 2009.

[9] G. D. Spiers *et al.*, "Atmospheric CO_2 measurements with a 2 μm airborne laser absorption spectrometer employing coherent detection, *Appl. Opt.*, vol. 50, no. 14, pp. 2098–2111, 2011.

[10] R. A. Robinson *et al.*, "First measurements of a carbon dioxide plume from an industrial source using a ground based mobile differential absorption lidar, *Environ. Sci.: Processes Impacts* vol. 16, pp. 1957–1966, 2014.

[11] T. F. Refaat *et al.*, "Evaluation of an airborne triple-pulsed 2μm IPDA lidar for simultaneous and independent atmospheric water vapor and carbon dioxide measurements," *Appl. Opt.*, vol. 54, pp. 1387–1398, 2015.

[12] F. Gibert, D. Edouart, and C. Cénac, "2-μm high-power multiple frequency single-mode Q-switched Ho:YLF laser for DIAL application, *Appl. Phys. B*, vol. 116, pp. 967–976, 2014.

[13] F. Gibert *et al.*, "2-μm Ho emitter-based coherent DIAL for CO_2 profiling in the atmosphere, *Opt. Lett.* vol. 40, pp. 3093–3096, 2015.

[14] S. Kameyama *et al.*, "Development of 1.6 μm continuous-wave modulation hard-target differential absorption lidar system for CO_2 sensing, *Opt. Lett.*, vol. 34, no. 10, pp. 1513–1515, 2009.

[15] J. B. Abshire *et al.*, "Pulsed airborne lidar measurements of atmospheric CO_2 column absorption, *Tellus B Chem. Phys. Meterol.*, vol. 62, no. 5, pp. 770–783, 2010.

[16] W. Johnson, K. S. Repasky, and J. L. Carlsten, "Micropulse differential absorption lidar for identification of carbon sequestration site leakage," *Appl. Opt.*, vol. 52, pp. 2994–3003, 2013.

[17] J. T. Dobler *et al.*, "Atmospheric CO_2 column measurements with an airborne intensity-modulated continuous wave 1.57 μm fiber laser lidar," *Appl. Opt.*, vol. 52, no. 12, pp. 2874–2892, Apr 2013.

[18] M. Queißer, M. Burton, and L. Fiorani, "Differential absorption lidar for volcanic CO_2 sensing tested in an unstable atmosphere, *Opt. Express*, vol. 23, pp. 6634-6644, 2015.

[19] A. W. Yu *et al.*, "Laser amplifier development for IPDA Lidar measurements of CO2 from space," in *Proc. SPIE* 9342, Solid State Lasers XXIV: Technology and Devices, 93420M (February 20, 2015); doi:10.1117/12.2080792.

[20] S. Gupta *et al.*, "Development, testing, and initial space qualification of 1.5-m, high-power (6 W), pulse-position-modulated fiber laser transmitter for deep-space laser communication," *Opt. Eng.*, vol. 55, no. 11, p. 111606, 2016.

[21] M. Storm *et al.*, "Space-Based Erbium-Doped Fiber Amplifier Transmitters for Coherent, Ranging, 3D-Imaging, Altimetry, Topology, and Carbon Dioxide Lidar and Earth and Planetary Optical Laser Communications," *EPJ Web of Conferences*, vol. 119, p.02002, 2016.

[22] G. A. Wagner and D. F. Plusquellic, "Ground-based, integrated path differential absorption LIDAR measurement of CO_2, CH_4, and H_2O near 1.6μm," *Appl. Opt.*, vol. 55, pp. 6292–6310, 2016.

[23] H. Wenzel *et al.*, "High peak power optical pulses generated with a monolithic master-oscillator power amplifier," *Opt. Lett.*, vol. 37, no. 11, pp. 1826–1828, Jun 2012.

[24] P. Adamiec *et al.*, "High-peak-power pulse generation from a monolithic master oscillator power amplifier at 1.5 μm," *Appl. Opt.*, vol. 51, no. 30, pp. 7160–7164, Oct 2012.

[25] M.-C. Amann, T. Bosch, M. Lescure, R. Myllyla, and M. Rioux, "Laser ranging: a critical review of usual techniques for distance measurement," *Opt. Eng.*, vol. 40, no. 1, pp. 10–19, 2001.

[26] O. Batet, F. Dios, A. Comeron, and R. Agishev, "Intensity-modulated linear-frequency-modulated continuous-wave lidar for distributed media: fundamentals of technique," *Appl. Opt.*, vol. 49, no. 17, pp. 3369–3379, Jun 2010.

[27] N. Takeuchi, N. Sugimoto, H. Baba, and K. Sakurai, "Random modulation cw lidar," *Appl. Opt.*, vol. 22, no. 9, pp. 1382–1386, May 1983.

[28] M. Imaki *et al.*, "Laser absorption spectrometer using frequency chirped intensity modulation at 1.57 μm wavelength for CO_2 measurement," *Opt. Lett.*, vol. 37, no. 13, pp. 2688–2690, Jul 2012.

[29] J. F. Campbell, B. Lin, and A. R. Nehrir, "Advanced sine wave modulation of continuous wave laser system for atmospheric CO_2 differential absorption measurements," *Appl. Opt.*, vol. 53, no. 5, pp. 816–829, Feb 2014.

[30] J. F. Campbell, B. Lin, A. R. Nehrir, F. W. Harrison, and M. D. Obland, "Super-resolution technique for CW lidar using Fourier transform reordering and Richardson-Lucy deconvolution," *Opt. Lett.*, vol. 39, no. 24, pp. 6981–6984, Dec 2014.

[31] J. F. Campbell, B. Lin, A. R. Nehrir, F. W. Harrison, and M. D. Obland, "Binary phase shift keying on orthogonal carriers for multi-channel CO_2 absorption measurements in the presence of thin clouds," *Opt. Express*, vol. 22, no. S6, pp. A1634–A1640, Oct 2014.

[32] B. Lin *et al.*, "Atmospheric CO_2 column measurements in cloudy conditions using intensity-modulated continuous-wave lidar at 1.57 micron," *Opt. Express*, vol. 23, no. 11, pp. A582–A593, Jun 2015.

[33] X. Ai, R. Nock, J. G. Rarity, and N. Dahnoun, "High-resolution random-modulation cw lidar," *Appl. Opt.*, vol. 50, no. 22, pp. 4478–4488, Aug 2011.

[34] Z. Yang, C. Li, M. Yu, F. Chen, and T. Wu, "Compact 405-nm random-modulation continuous wave lidar for standoff biological warfare detection," *J. Appl. Remote Sens.*, vol. 9, no. 1, p. 096042, 2015.

[35] R. Matthey and V. Mitev, "Pseudo-random noise-continuous-wave laser radar for surface and cloud measurements," *Opt. Laser Eng.*, vol. 43, no. 35, pp. 557 – 571, 2005.

[36] B. Cochenour, L. Mullen, and J. Muth, "Modulated pulse laser with pseudorandom coding capabilities for underwater ranging, detection, and imaging," *Appl. Opt.*, vol. 50, no. 33, pp. 6168–6178, Nov 2011.

[37] C.-Y. She *et al.*, "Mesopause-region temperature and wind measurements with pseudorandom modulation continuous-wave (PMCW) lidar at 589 nm," *Appl. Opt.*, vol. 50, no. 18, pp. 2916–2926, Jun 2011.

[38] J. A. R. Rall, J. B. Abshire, D. Reusser and M. Humphrey, "Measurements of atmospheric water vapor using a compact AlGaAs laser based DIAL instrument," in *Conference on Lasers and Electro-Optics*, 1994.

[39] C. M. Gittins *et al.*, "Quantitative gas sensing by backscatter-absorption measurements of a pseudorandom code modulated $\lambda \sim$ 8-μm quantum cascade laser," *Opt. Lett.*, vol. 25, no. 16, pp. 1162–1164, Aug 2000.

[40] M. Faugeron *et al.*, "High power three-section integrated master oscillator power amplifier at 1.5 μm," *IEEE Photon. Technol. Lett.*, vol. 27, no. 13, pp. 1449–1452, July 2015.
[41] X. Ai *et al.*, "Pseudo-random single photon counting for space-borne atmospheric sensing applications," in *2014 IEEE Aerospace Conference*, March 2014.
[42] R. T. Menzies and D. M. Tratt, "Differential Laser absorption spectrometry for global profiling of tropospheric carbon dioxide: selection of optimum sounding frequencies for high-precision measurements," *Appl. Opt.* vol. 42, pp. 6569–6577, 2003.
[43] J. Caron and Y. Durand, "Operating wavelengths optimization for a spaceborne lidar measuring atmospheric CO_2," *Appl. Opt.* vol. 48, pp. 5413–5422, 2009.
[44] X. Ai *et al.*, "Analysis of a pseudo-random single photon counting differential absorption lidar system for space-borne atmospheric CO_2 sensing," *Opt. Express*, vol. 24, no. 18, pp. 21119–21133, Sept 2016.
[45] J. F. Campbell, N. S. Prasad and M. A. Flood, "Pseudorandom noise code-based technique for thin-cloud discrimination with CO_2 and O_2 absorption measurements," *Opt. Eng.*, vol. 50, no. 12, pp. 126002–126002-8, 2011.
[46] J. F. Campbell, N. S. Prasad, F. W. Harrison and M. A. Flood, "Time shifted PN codes for CW LiDAR, radar, and sonar," U.S. Patent 8 605 262, Dec 29, 2011.
[47] J. G. Rarity *et al.*, "Single-photon counting for the 1300–1600-nm range by use of peltier-cooled and passively quenched InGaAs avalanche photodiodes," *Appl. Opt.*, vol. 39, no. 36, pp. 6746–6753, Dec 2000.
[48] B. O. Bundschuh, D. Schneider, and M. Grindel, "Feasibility study of a compact low cost correlation lidar using a pseudo noise modulated diode laser and an APD in the current mode," in *Geoscience and Remote Sensing Symposium, 1996. IGARSS '96. 'Remote Sensing for a Sustainable Future.', International*, vol. 2, May 1996, pp. 999–1001 vol.2.
[49] M. Quatrevalet *et al.*, "CHARM-F: The airborne integral path differential absorption lidar for simultaneous measurements of atmospheric CO_2 and CH_4," *in Proceedings of the 25th International Laser Radar Conference (ILRC 25)*, 2010.
[50] A. Fix *et al.*, "Development and first results of a new near-ir airborne greenhouse gas lidar," in *Advanced Solid State Lasers*. Optical Society of America, 2015, p. ATh1A.2.
[51] L. Rothman *et al.*, "The HITRAN2012 molecular spectroscopic database," *J. Quant. Spectrosc. Radiat. Transfer*, vol. 130, pp. 4 – 50, 2013.

Mathieu Quatrevalet was born in Creutzwald, France, in 1980. He graduated as an optical engineer from the Institut d'Optique Graduate School in Palaiseau, France in 2004. He worked on performance simulations and requirements definitions for both passive and active earth observation instruments at ESA's European Space Research and Technology Centre from 2004 to 2007, and operated and upgraded a combined aerosol and ozone lidar managed by the Service d'Aéronomie (now Laboratoire Atmosphères, Milieux, Observations Spatiales, LATMOS) at the French Antarctic polar station Dumont d'Urville, in the frame of a winter over in 2008. Since 2009 he is with DLR's Institute of Atmospheric Physics, working on the development of air-borne and space-borne lidars for trace gas measurements.

Xiao Ai is a postdoctoral researcher at University of Bristol, graduated from his PhD program which specialized in 3D imaging techniques. His research involves the development of lidar technologies: for remote sensing and range finding applications. Xiao also has extensive experience on optoelectronic systems, analogue and digital signal processing.

Antonio Pérez-Serrano was born in Badalona, Spain, in 1978. He graduated and obtained the Ph.D. in Physics from the Universitat de les Illes Balears, Palma de Mallorca, Spain, in 2006 and 2011, respectively. He is currently a research associate at the Universidad Politécnica de Madrid, Spain. His research interests include semiconductor laser modeling and dynamics, with particular emphasis in multimode dynamics, non-linear dynamics and high-power semiconductor lasers. He is also interested in remote sensing applications such as lidar systems for gas concentration and distance measurements.

Pawel Adamiec received the M.Sc. degree in physics and computer sciences from Rzeszow Pedagogical University, Poland, in 2000 and Ph.D. degree in physics from Warsaw University of Technology, Poland, in 2006. From 2000 to 2012 he was investigating the properties of the semiconductor lasers and other optoelectronic devices. Since 2014 he has engaged in the analysis and studies of new photonic technologies for the aerospace sector at ALTER Technology. He is an author or co-author of more than 50 peer-reviewed journal papers and conference contributions.

Juan Barbero was born in Segovia, Spain in 1968. He received the M.S. degree in Material Physics from the Universidad Complutense de Madrid in 1991. From 1991 to 1997, he was a Technical analyzer at the Failure Analysis Laboratory of Alcatel in Madrid. From 1997 to 2002 he worked in the Central Quality Laboratory of Alcatel. Since 2002, he has been involved in the Innovation Area of ALTER Technology (former Tecnologica). His areas of interest include Optoelectronic technologies and development of non-standard test setups for testing components for space applications.

Andreas Fix graduated at University of Hannover, Germany in co-operation with Laser Zentrum Hannover. In 1995 he received the Ph.D. degree in Physics from University of Kaiserslautern, Germany, with an experimental work on laser physics and nonlinear optics. He joined DLR, first as a post doctoral researcher, later as a research scientist and since then is engaged in the development and application of ground-based, airborne and spaceborne lidar systems.

Jose Manuel G. Tijero was born in Burgos, Spain, in 1960. He received the M.Sc. and Ph.D degrees in physics from the Universidad de Zaragoza in 1984 and from the Universidad Autónoma de Madrid in 1989, respectively. His research activity has included the spectroscopic study of defects in ionic crystals, the optoelectronic characterization of SiGe/Si heterostructures, and the study of InGaAs/GaAs lasers and quantum well infrared detectors. His current research interest focuses on the modeling, simulation and characterization of laser diodes for high-power applications. Since 1994, he is an Associate Professor at the Universidad Politécnica de Madrid.

Ignacio Esquivias was born in Madrid, Spain, in 1955. He received the M.Sc. and Ph.D. degrees in Electronic Engineering from the Universidad Politécnica de Madrid in 1977 and 1983, respectively, becoming Full Professor at this university in 2001. He leads the Laser Diode Group of the CEMDATIC, with activity in laser diode modeling and characterization since 1992. He has been PI in 10 national and 5 EC funded international projects on laser diodes, and he has published more than 100 journal and conference papers on this field.

John G. Rarity is professor of optical communication systems in the Dept. of Electrical and Electronic Engineering at the University of Bristol, a post he has held since 2003. He is a member of the Quantum Computation and Information group and quantum photonics at the University of Bristol. He was elected a Fellow of the Royal Society (FRS) in 2015.

Gerhard Ehret was born in Kenzingen, Germany, in 1953. He received his diploma in Physics and became Dr.rer.net at the University Freiburg, Germany, in 1981 and 1986, respectively. Since 1986, he has served in numerous research roles to apply lidar in atmospheric studies at DLR Oberpfaffenhofen, Germany. He was member of the WALES and A-SCOPE Mission Advisory Groups at ESA, and is currently the Co-Principal Investigator of the French-German climate mission MERLIN. Since 2000, he has served as Head of the LIDAR Department at the Institute for Atmospheric Physics at DLR Oberpfaffenhofen, Germany.